Cell Reports, Volume *43*

Supplemental information

Molecular cascade reveals sequential milestones underlying hippocampal neural stem cell development into an adult state

Dennisse Jimenez-Cyrus, Vijay S. Adusumilli, Max H. Stempel, Sandra Maday, Guo-li Ming, Hongjun Song, and Allison M. Bond

SUPPLEMENTARY FIGURES

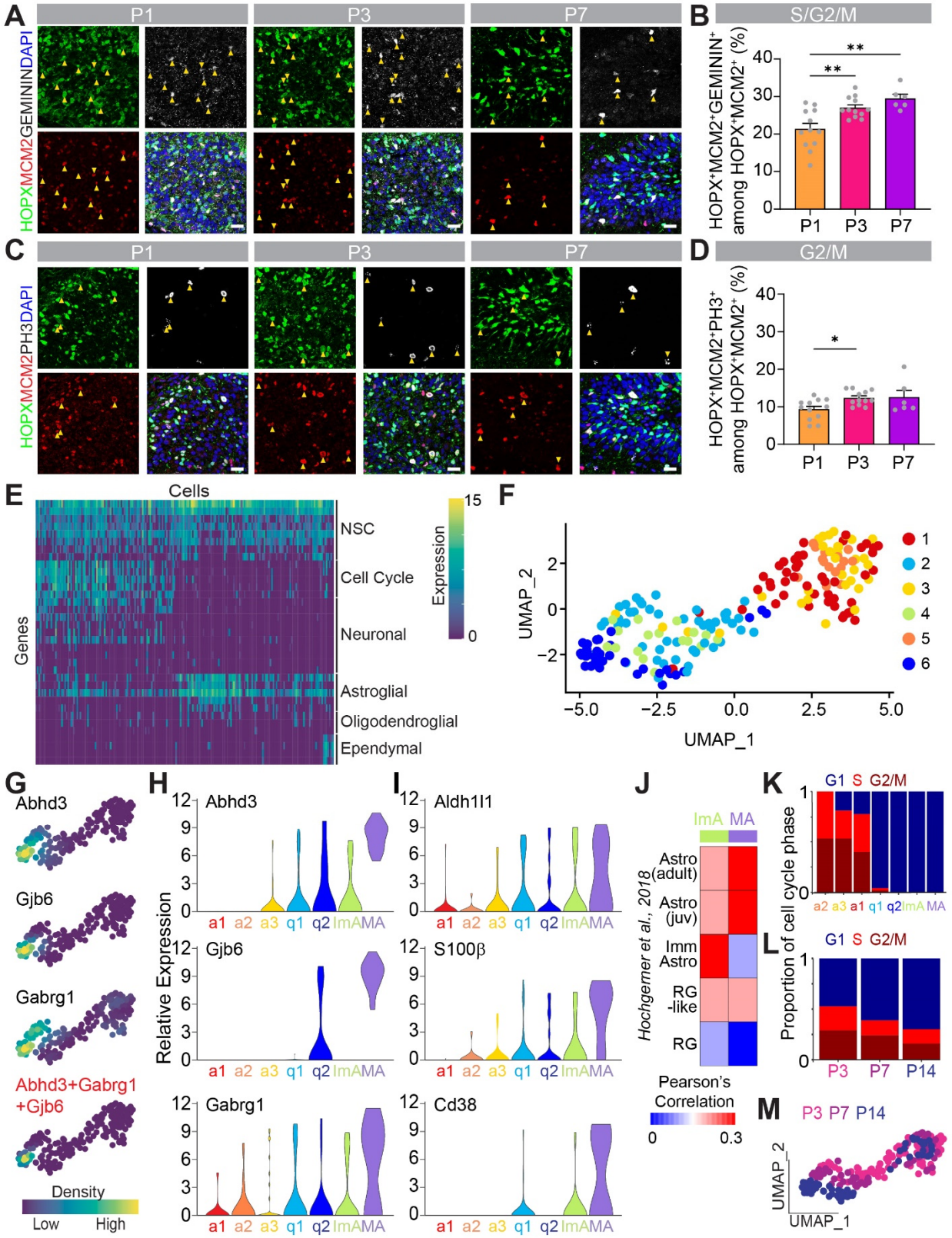

Figure S1. Cell Cycle Changes and Multiple Transcriptional States of Neural Stem Cells During Early Postnatal Development, related to Figure 1

(A) Sample confocal images of $HOPX^+MCM2^+GEMININ^+$ dentate gyrus (DG) neural stem cells (NSCs) at P1, P3, and P7. Yellow arrowheads point to triple-positive cells. Scale bars, 20 μm.
(B) Quantification of the percentage of $HOPX^+MCM2^+GEMININ^+$ cells among all dividing $HOPX^+MCM2^+$ cells in the DG. The same P1, P3 and P7 mice in Figure 1B were used. Values represent mean ± SEM (n = 6-12 mice; $^{**}p < 0.01$; one-way ANOVA with Tukey's post hoc test).
(C) Sample confocal images of $HOPX^+MCM2^+PH3^+$ DG NSCs at P1, P3, and P7. Yellow arrows point to triple-positive cells. Scale bars, 20 μm.
(D) Quantification of the percentage of $HOPX^+MCM2^+PH3^+$ cells among all dividing $HOPX^+MCM2^+$ cells in the DG. The same P1, P3 and P7 mice in Figure 1B were used. Values represent mean ± SEM ($^*p < 0.05$; one-way ANOVA with Tukey's post hoc test).
(E) Heatmap of cell type-specific gene expression (y-axis) of all sequenced cells (x-axis).
(F) UMAP of 189 cells (excluding ependymal cells) separated into 6 clusters identified using unsupervised Monocle2 clustering.
(G) Kernel density estimation plots showing the distribution of mature astrocyte gene expression (top 3 panels) used to create an astrocyte score (bottom panel) in each cell on the UMAP.
(H-I) Violin plots of expression of genes used to create the mature astrocyte score (H) and of additional astrocyte-specific genes (I) for each cluster (a1, active-1; a2, active-2; a3, active-3; q1, quiescent-1; q2, quiescent-2; ImA, immature astrocyte; MA, mature astrocyte).
(J) Gene expression correlation plot of the ImA and MA clusters from our dataset (x-axis) compared to astroglial and NSC clusters from a previously published single-cell RNA-sequencing dataset from mouse DG (y-axis; Hochgerner et al., 2018)[1].
(K) Bar plot of cell cycle phase (G1, S, G2/M) distribution in each cluster.
(L) Bar plot of cell cycle phase (G1, S, G2/M) distribution at each age.
(M) UMAP of each cell showing its age (P3, P7, P14).

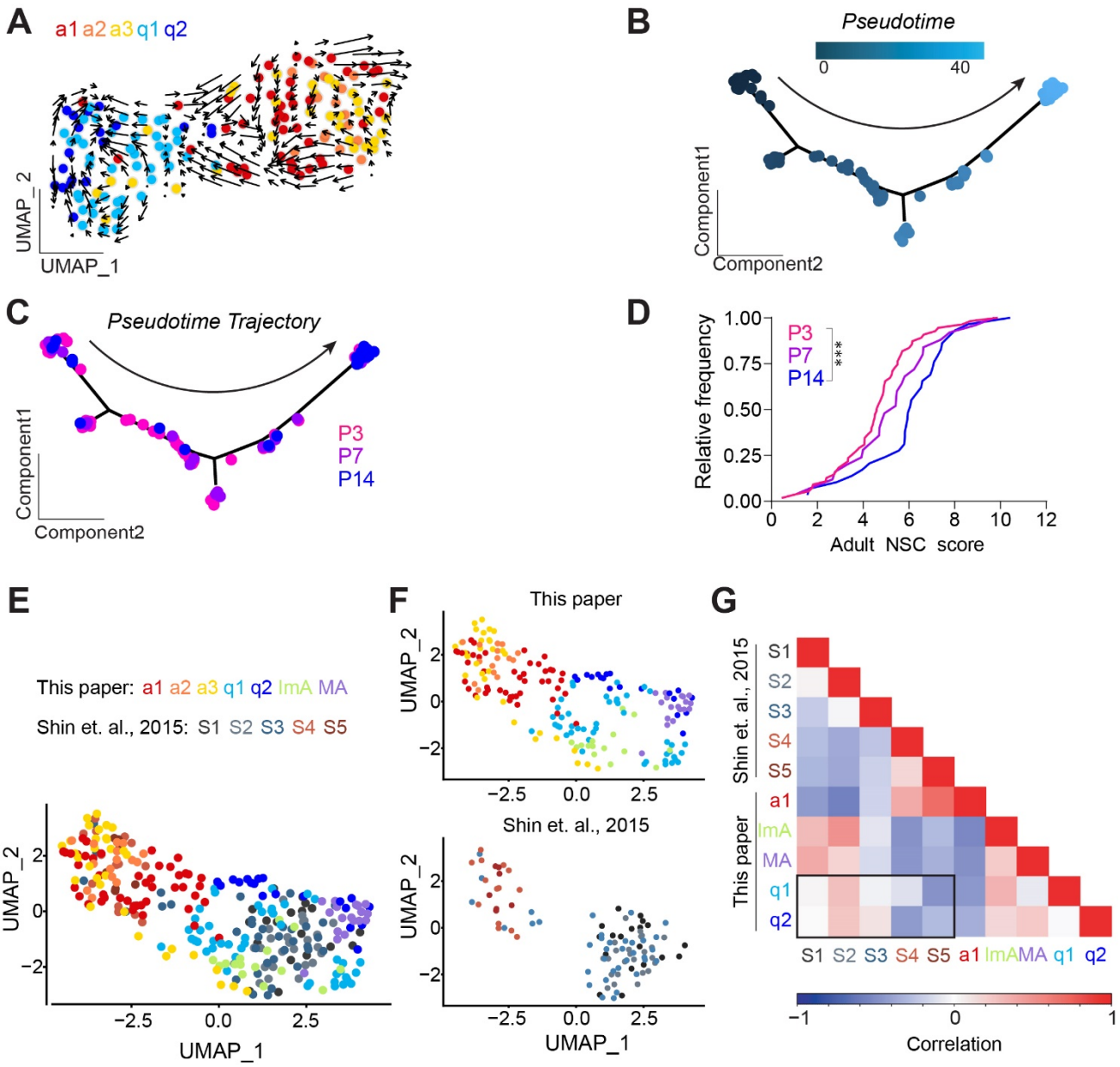

Figure S2. Single-Cell RNA-Sequencing Reveals a Trajectory Representing the Neural Stem Cell Transition into an Adult State, related to Figure 2

(A) UMAP of cells in Figure 2A with astroglial lineage cells (ImA, immature astrocytes and MA, mature astrocytes) removed. RNA velocity analysis shows the predicted future state of cells overlaied on the cluster UMAP.

(B) Principal component analysis (PCA) of each cell from clusters a1, q1 and q2 showing its pseudotime value in the pseudotime trajectory that represents the NSC transition to a quiescent adult state. Arrow indicates direction of the pseudotime trajectory.

(C) PCA of each cell from clusters a1, q1 and q2 showing its age (P3, P7, P14) in the pseudotime trajectory that represents the NSC transition to a quiescent adult state.

(D) Distribution curve of Adult NSC Scores for individual cells from ages P3, P7, and P14. Note the gradual change in adult NSC gene expression from P3 to P7 and P7 to P14 (***$p < 0.001$; Kruskal-Wallis rank sum test with Dunn's post hoc test).

(E-F) UMAP of cells from this early postnatal dataset (a1, active-1; a2, active-2; a3, active-3; q1, quiescent-1; q2, quiescent-2; ImA, immature astrocyte; MA, mature astrocyte) and cells from an

adult NSC and progenitor dataset[2] (S1-S5) shown as an integrated UMAP (E) or separated by dataset (F).
(G) Gene expression correlation plot of the trajectory clusters (a1, q1 and q2) and the astroglial clusters (ImA and MA) from this dataset compared to clusters from and adult NSC dataset[2] (S1-5).

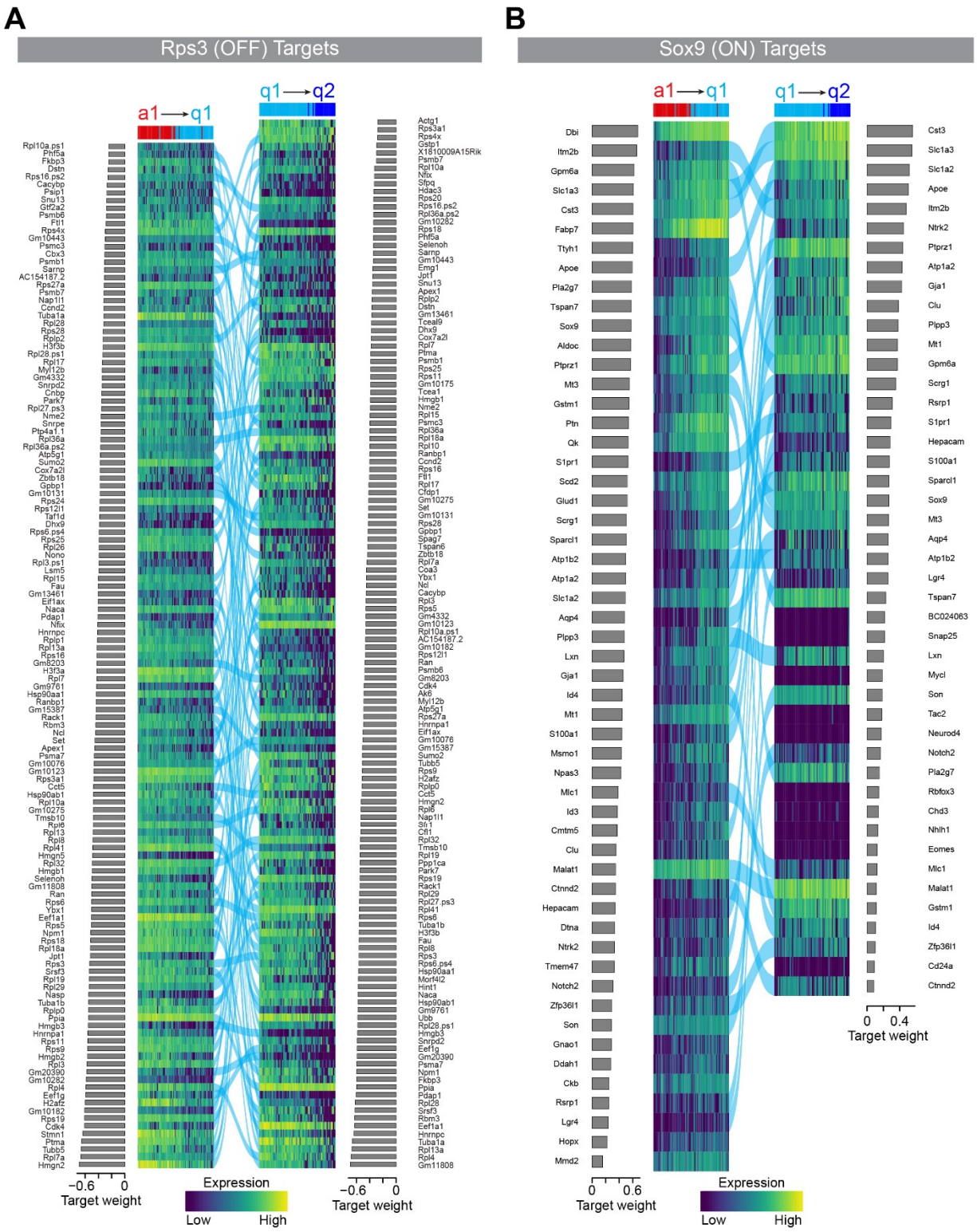

Figure S3. Gene Regulatory Network Analysis Reveals a Distinct Complement of Target Genes for the Same Regulon at Each Step of Neural Stem Cell Development, related to Figure 3

(A) Heatmap of the Rps3 regulon's target genes' expression across the a1 to q1 step (left panel) and q1 to q2 step (right panel) of the pseudotime trajectory. Blue lines show common targets of

Rps3 in both steps of the pseudotime trajectory. Target genes are in order of Target Weight (bar plots), a measure of their contribution to the regulon in each step of the pseudotime trajectory. (B) Heatmap of the Sox9 regulon's target genes' expression across the a1 to q1 step (left panel) and q1 to q2 step (right panel) of the pseudotime trajectory. Blue lines show common targets of Sox9 in both steps of the pseudotime trajectory. Target genes are in order of Target Weight (bar plots), a measure of their contribution to the regulon in each step.

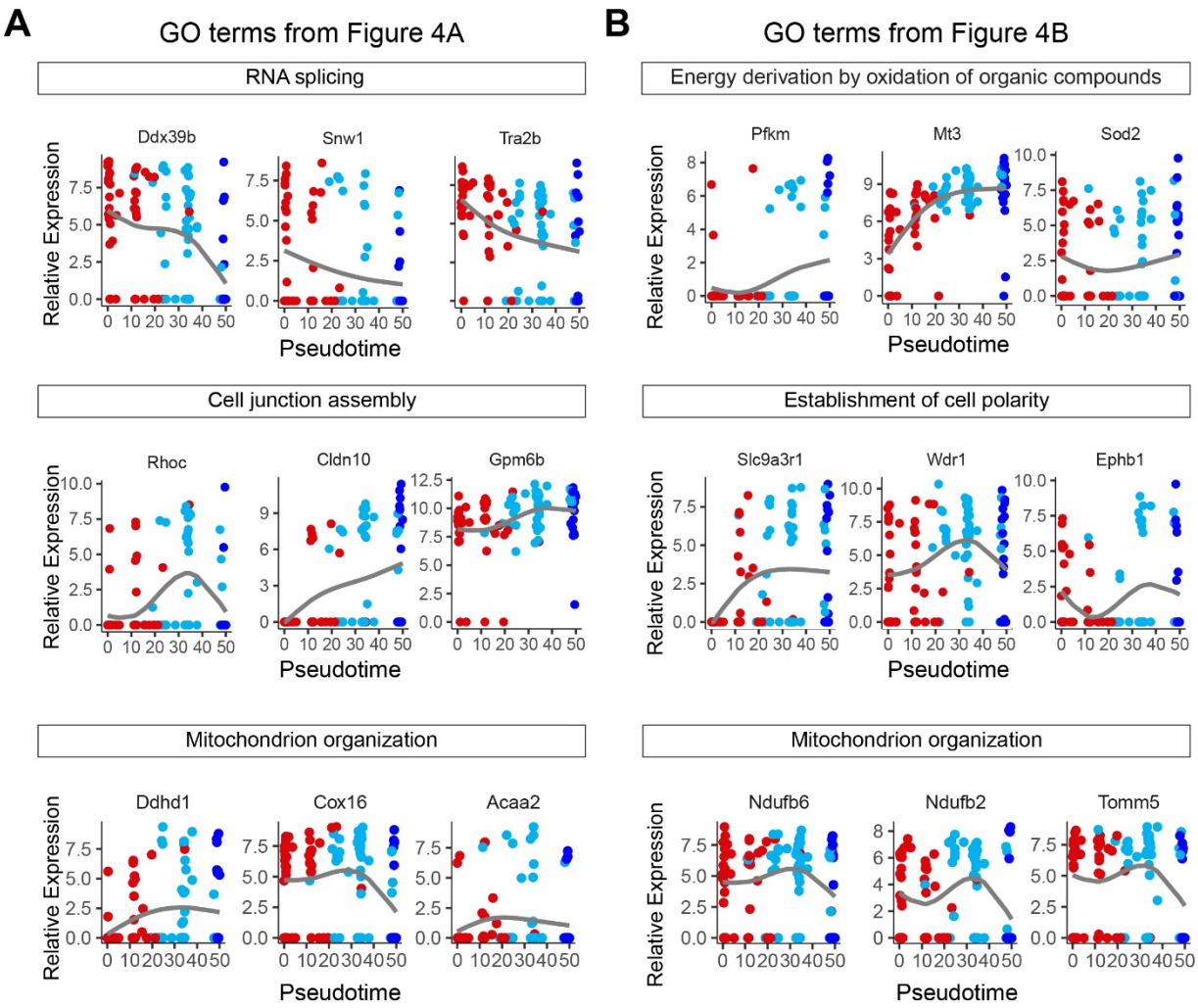

Figure S4. Gene Ontology Analysis Reveals Cell Biology Underlying the Neural Stem Cell Transition into an Adult State, related to Figure 4

(A) Dot plot of example genes from GO terms highlighted in red in Figure 4A (RNA splicing, Cell junction assembly, Mitochondrion organization) in individual cells (a1, red; q1, light blue; q2, dark blue) across the pseudotime.

(B) Dot plot of example genes from GO terms highlighted in red in Figure 4B (Energy derivation by oxidation of organic compounds, Establishment of cell polarity, Mitochondrion organization) in individual cells (a1, red; q1, light blue; q2, dark blue) across the pseudotime.

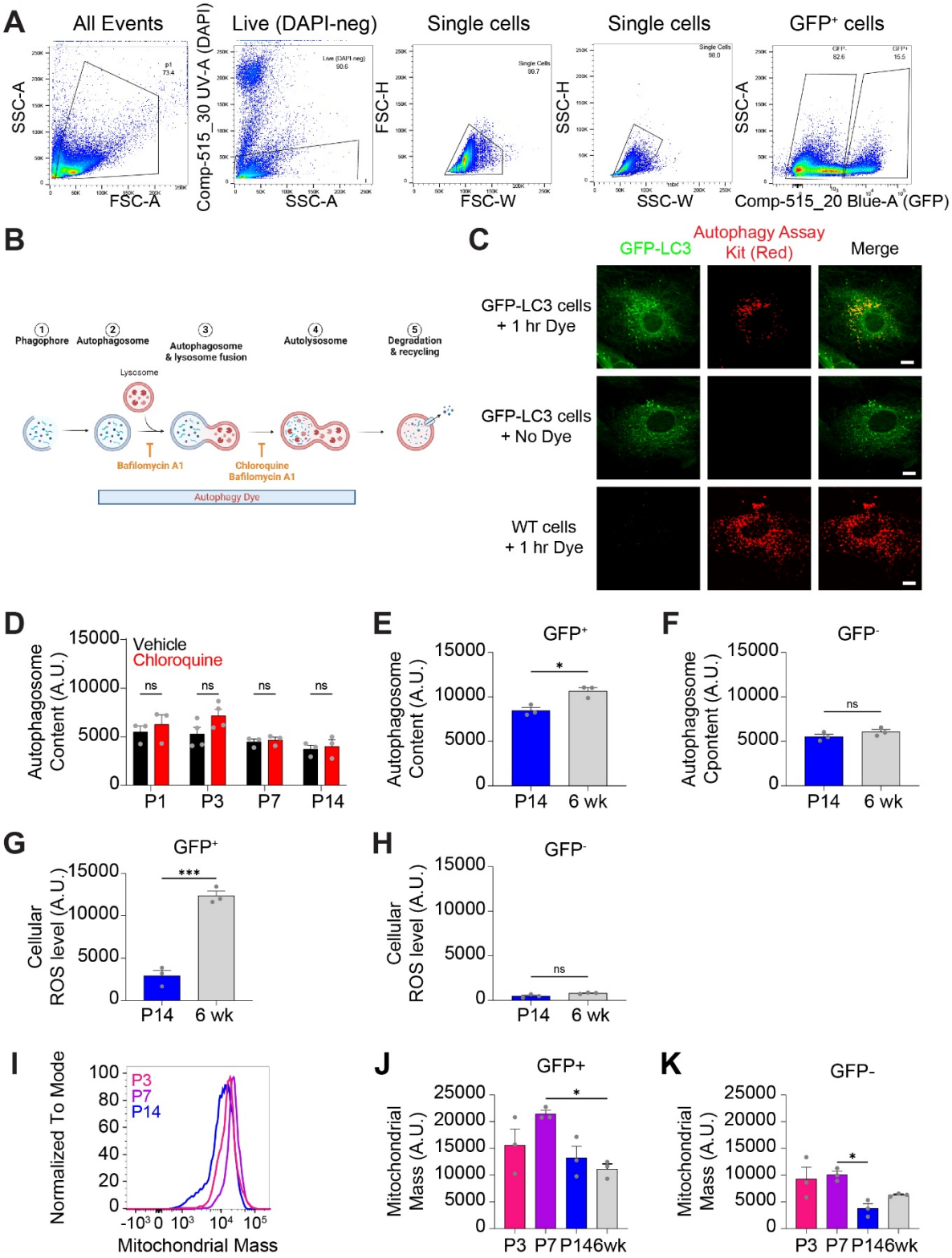

Figure S5. Flow Cytometric Analysis of Metabolism During Neural Stem Cell Development into a Quiescent Adult State, related to Figure 5.

(A) Flow cytometry gating scheme for GFP⁺ and GFP⁻ cells.

(B) Schematic illustration of the autophagy process, the steps of the process labeled by Autophagy Assay Kit (Red), and the steps of the process blocked by the inhibitors, chloroquine and bafilomycin A1.
(C) Confocal images of *in vitro* astrocyte cultures from *GFP-LC3* mice incubated with Autophagy Assay Kit (Red) for 1 hour (top panel) or incubated without the dye (middle panel), as well as *in vitro* astrocyte cultures from wildtype mice incubated with Autophagy Assay Kit (Red) for 1 hour (bottom panel). Autophagy Assay Kit (Red) puncta colocalize with most GFP^+ puncta in *GFP-LC3* mice and no bleed through is observed in the green or red channel in single conditions. Scale bars: 10 μm.
(D) Flow cytometry analysis of autophagic vesicle content in GFP^- cells from the DG of P1, P3, P7, and P14 *Hopx-3xFlag-GFP* mice after vehicle or chloroquine treatment shown as an average of all samples. Values represent mean ± SEM (n = 3 experiments; 3 mice were pooled for each experimental sample; ns: $p > 0.05$; two-way ANOVA with Šídák's multiple comparisons test).
(E) Flow cytometry analysis of autophagic vesicle content in GFP^+ cells from the DG of P14 and 6 week *Hopx-3xFlag-GFP* mice shown as an average of all samples. The same P14 data was used in Figure 5D. Values represent mean ± SEM (n = 3 experiments; 3 mice were pooled for each experimental sample; *$p < 0.05$; unpaired t-test).
(F) Flow cytometry analysis of autophagic vesicle content in GFP^- cells from the DG of P14 and 6 week *Hopx-3xFlag-GFP* mice shown as an average of all samples. The same P14 data was used in Figure 5E. Values represent mean ± SEM (n = 3 experiments; 3 mice were pooled for each experimental sample; ns: $p > 0.05$; unpaired t-test).
(G) Flow cytometry analysis of cellular ROS levels in GFP^+ cells from the DG of P14 and 6 week *Hopx-3xFlag-GFP* mice shown as an average of all samples. The same P14 data was used in Figure 5K. Values represent mean ± SEM (n = 3 experiments; 3 mice were pooled for each experimental sample; ***$p < 0.001$; unpaired t-test).
(H) Flow cytometry analysis of cellular ROS levels in GFP^- cells from the DG of P14 and 6 week *Hopx-3xFlag-GFP* mice shown as an average of all samples. The same P14 data was used in Figure 5L. Values represent mean ± SEM (n = 3 experiments; 3 mice were pooled for each experimental sample; ns: $p > 0.05$; unpaired t-test).
(I-K) Flow cytometry analysis of mitochondrial mass in GFP^+ cells (I-J) and GFP^- cells (K) from the DG of P3, P7, and P14 *Hopx-3xFlag-GFP* mice using MitoTraker™ Deep Red. Mitochondrial mass in GFP^+ NSCs shown as a histogram of individual samples (I) and a bar plot of the average of all samples (J), as well as mitochondrial mass of GFP^- cells shown as a bar plot of the average of all samples (K). Values represent mean ± SEM (n = 3 experiments; 3 mice were pooled for each experimental sample; *$p < 0.05$; one-way ANOVA with Tukey's post hoc test).

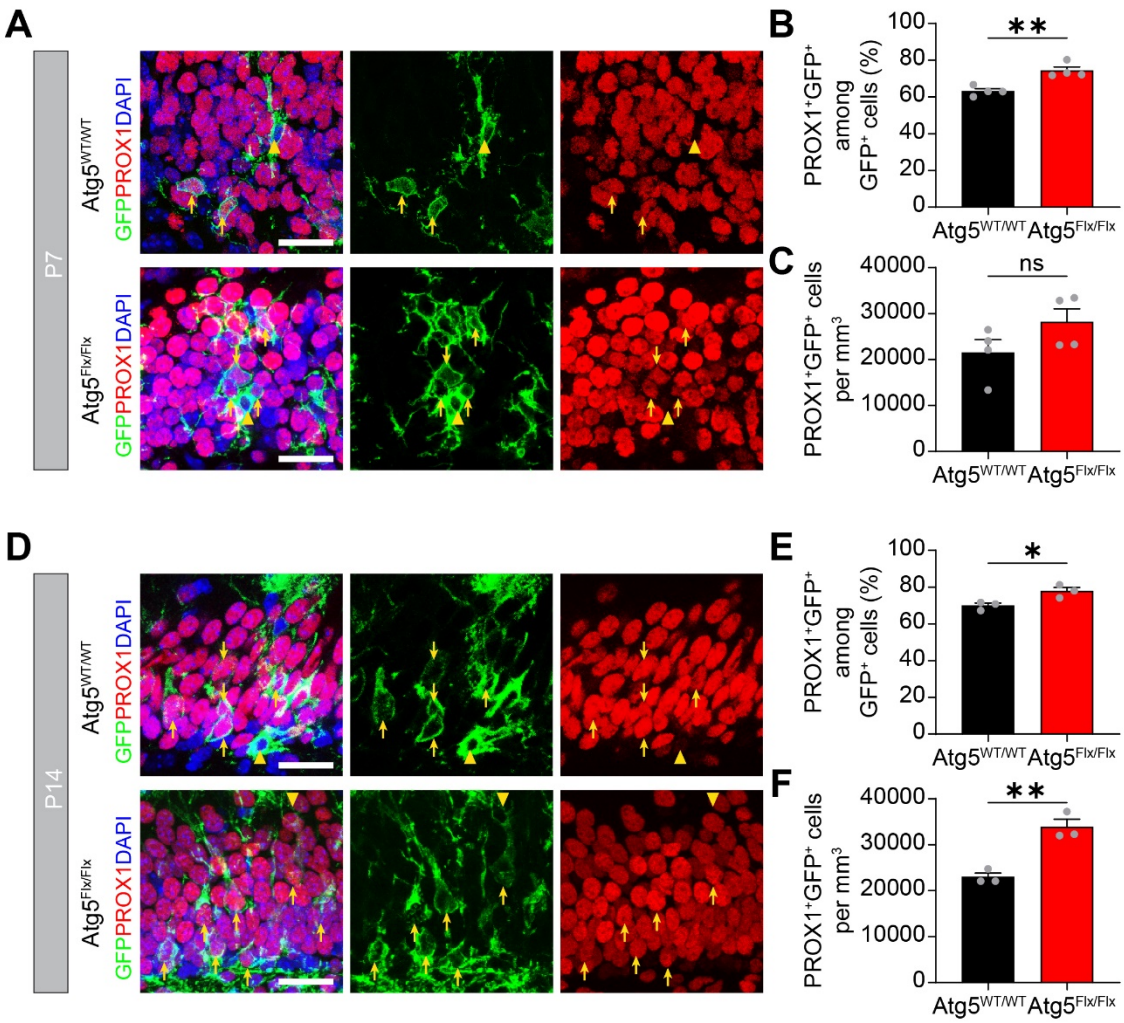

Figure S6. Autophagy Inhibition Dysregulates Early Postnatal Neurogenesis, related to Figure 6.

(A) Sample confocal images of DG neurons (GFP$^+$PROX1$^+$) at P7 generated from HOPX$^+$ recombined cells at P1 in *Hopx-CreER^{T2}::mTmG Atg5$^{WT/WT}$* and *Hopx-CreER^{T2}::mTmG Atg5$^{Flx/Flx}$* mice. Yellow arrows indicate GFP$^+$PROX1$^+$ neurons and yellow arrowheads indicate GFP$^+$PROX1$^-$ non-neuronal cells. Scale bars, 25 μm.

(B) Quantification of the percentage of PROX1$^+$ cells among all GFP$^+$ cells in the DG at P7. Each dot represents data from one mouse. Values represent mean ± SEM (n = 4 mice; **p < 0.01; unpaired t-test).

(C) Quantification of the number of GFP$^+$PROX1$^+$ neurons in the DG at P7. Each dot represents data from one mouse. Values represent mean ± SEM (n = 4 mice; ns: p > 0.05).

(D) Sample confocal images of DG neurons (GFP$^+$PROX1$^+$) at P14 generated from HOPX$^+$ recombined cells at P1 in *Hopx-CreER^{T2}::mTmG Atg5$^{WT/WT}$* and *Hopx-CreER^{T2}::mTmG Atg5$^{Flx/Flx}$* mice. Yellow arrows indicate GFP$^+$PROX1$^+$ neurons and yellow arrowheads indicate GFP$^+$PROX1$^-$ non-neuronal cells. Scale bars, 25 μm.

(E) Quantification of the percentage of PROX1$^+$ cells among all GFP$^+$ cells in the DG at P14. Each dot represents data from one mouse. Values represent mean ± SEM (n = 4 mice; *p < 0.05; unpaired t-test).

(F) Quantification of the number of GFP$^+$PROX1$^+$ neurons in the DG at P14. Each dot represents data from one mouse. Values represent mean ± SEM (n = 4 mice; **p < 0.01; unpaired t-test).

SUPPLEMENTAL REFERENCES

1. Hochgerner, H., Zeisel, A., Lönnerberg, P., and Linnarsson, S. (2018). Conserved properties of dentate gyrus neurogenesis across postnatal development revealed by single-cell RNA sequencing. Nat Neurosci 21, 290–299. 10.1038/s41593-017-0056-2.

2. Shin, J., Berg, D.A., Zhu, Y., Shin, J.Y., Song, J., Bonaguidi, M.A., Enikolopov, G., Nauen, D.W., Christian, K.M., Ming, G., et al. (2015). Single-Cell RNA-Seq with Waterfall Reveals Molecular Cascades underlying Adult Neurogenesis. Cell Stem Cell 17, 360–372. 10.1016/j.stem.2015.07.013.